PCCP

Accepted Manuscript

ROYAL SOCIETY OF CHEMISTRY

www.rsc.org/pccp

Cite this: DOI: 10.1039/c0xx00000x

www.rsc.org/xxxxxx

ARTICLE TYPE

Hydrogen storage in platinum decorated Hydrogen Exfoliated Graphene sheets by spillover mechanism

Divya P. and S. Ramaprabhu

Received (in XXX, XXX) Xth XXXXXXXXX 20XX, Accepted Xth XXXXXXXXX 20XX

DOI: 10.1039/b000000x

Development of light-weight materials with high hydrogen storage capacity is a great challenge in hydrogen economy. Here, we report high pressure hydrogen adsorption-desorption studies of platinum-hydrogen exfoliated graphene sheets (Pt-HEG). Pt-HEG shows a maximum hydrogen uptake capacity of 1.4 wt% at 25 °C and 3 MPa. Analysis of isosteric heat of adsorption provides evidence to spillover mechanism.

1. Introduction

Hydrogen is one of the energy sources for future by certain advantages such as abundance, easy synthesis and nonpolluting nature. Wide spread use of proton exchange membrane fuel cell for on board vehicular applications demand efficient and cost effective hydrogen storage methods. Commonly used methods for storing hydrogen are (1) Liquid hydrogen at very low temperatures (at 20 K for H_2), which suffers cost of liquefaction and boil off problem, (2) gas storage at extremely high pressures (200-300 atm), which raises safety concerns[1].

Hydrogen storage by adsorption is one potential strategy for effective and relatively safe hydrogen storage. An efficient hydrogen storage material must have high volumetric/ gravimetric capacity, fast sorption kinetics at relatively low temperatures, high tolerance to recycling and low cost [2]. Materials with large surface area and porosity can be good candidate for hydrogen storage. Carbon nanotubes, [3, 4] carbon nanofibers [5], activated carbon [6], metal-organic frameworks [7], and zeolites [8] have been studied as hydrogen storage material by their lightweight and high surface area.

Recently, graphene has received enthusiastic attention as a potential hydrogen adsorbent due to its high surface area and chemical stability. The maximum predicted theoretical gravimetric densities are up to 8 wt % .[9] Experimental and theoretical studies reveal that, hydrogen can absorb on graphene either by physisorption or by chemisorptions.[2, 10-21]. Chemical functionalization has been proposed to enhance the hydrogen uptake capacity of graphene at ambient conditions. Transition metal loaded graphene can improve the interaction between molecular hydrogen and graphene.[22-25] It has been demonstrated in experiments that palladium (Pd) or platinum (Pt) dispersed graphene can enhance the hydrogen uptake by spillover mechanism. [2, 26]. Further, Vinayan *et al*. studied the hydrogen storage in nitrogen doped graphene as well as palldium deocorated nitrogen doped graphene experimentally[27, 28]. Nachimuthu *et al.* investigated the hydrogen storage capacity of transition metal decorated boron doped graphene using first principle calculations[29] and Wu *et al*. investigated the spill over mechanism on boron doped graphene by DFT calculations[30].

In the present study, we have synthesized few layer graphene sheets by hydrogen exfoliation technique. Platinum nanoparticles are dispersed over hydrogen exfoliated graphene sheets by polyol reduction technique. High pressure hydrogen adsorption studies of the present material have been carried out by Sieverts' apparatus. Present study elucidates adsorption mechanism of hydrogen on platinum-hydrogen exfoliated graphene.

2. Materials

Commercial graphite (sigma aldrich, 99%) was used as the graphene precursor. sodium nitrate ($NaNO_3$, 99.5%), potassium permanganate ($KMnO_4$, 99.5%), concentrated sulphuric acid (H_2SO_4, 98%) and ethylene glycol were purchased from Rankem Chemicals, India. Hydrogen peroxide (H_2O_2, 30%) was purchased from S D Fine-Chem. Ltd., India. Hexachloro platinic acid hexahydrate was purchased from Rankem Chemicals, India. D. I. water was used for all reactions.

3. Materials synthesis

Graphitic oxide (GO) was synthesized from natural graphite by Hummers' method [31]. Initially, graphite powder (2g) was dispersed in conc. H_2SO_4 (46ml) under stirring in an ice bath. Thereafter, 1 g of $NaNO_3$ and 6 g $KMnO_4$ were added slowly. Then, ice bath was removed and the resulting product was stirred in room temperature. Then 92 ml of water was added to above mixture. After 15 min, 280 ml warm water (45-50°C) was poured to dilute the mixture. Further, 3% H_2O_2 was added, above mixture was turned in to yellow colour. Then, the mixture was filtered and washed with warm water. The residue was diluted further using water. The resulting product was centrifuged, decanted and vacuum dried.

HEG was synthesized by exfoliation of graphite oxide. Required amount of GO was sprinkled over a quartz boat and it was loaded to the centre of a quartz tube. Then the quartz tube was inserted in a tubular furnace. Both ends of the quartz tube were closed with coupling arrangements have gas flow provision. Argon was allowed about 15 minutes to create an inert environment. The temperature of the furnace was raised to 250

°C and hydrogen was allowed at this temperature for the exfoliation to happen. The resulting product was named as HEG.[32]

Then HEG was dispersed in EG by ultrasonication. Next, 1wt% aqueous solution of hexachloroplatinic acid was added drop by drop to the above suspension and it was stirred for 12 hours. Reduction was carried out at 130 °C for 4 hours. Finally, the suspension was washed filtered and dried in a vacuum oven. The final product was labeled as Pt-HEG.

4. Experimental methods

4.1 Characterization methods

Fourier transformed Infrared spectroscopy experiment was conducted by a Perkin Elmer FT-IR spectrometer. Raman spectroscopy was carried out on a WITec alpha 300 instrument (confocal Raman spectrometer) with an excitation source of Nd:YAG laser (532 nm). Powder X-ray diffraction (XRD) analysis was conducted using PANalytical X'PERT Pro X-ray Diffractometer with nickel-filtered Cu Kα radiation as the X-ray source. Field emission scanning electron microscopy (FESEM) was carried out on FEI QUANTA 3D instrument operated at 30 kV. Sample was supported on a carbon tape. Transmission electron microscopy (TEM) was carried with a TECNAI F 20 (S-Twin) microscope operating at 200 kV. Sample dispersed in ethanol by mild ultrasonication was drop casted onto thin film of carbon coated Cu grids and dried (SPI supplies, 200 meshes) was used for TEM analysis. X-ray photoelectron spectroscopy (XPS) analysis was performed by Specs spectrometer with polychromatic Mg Kα (1253.6 eV) as the photon source. The vacuum maintained was 10^{-10} Torr. Brunauer-Emmer-Teller surface area and pore size distribution were calculated using micromeritics ASAP 2020 physisorption analyzer.

4.2 Hydrogen adsorption isotherms measurement

Hydrogen adsorption studies at different temperatures and pressures were conducted using a Sieverts' apparatus. The instrument was assured leak free. About 100 mg of the sample

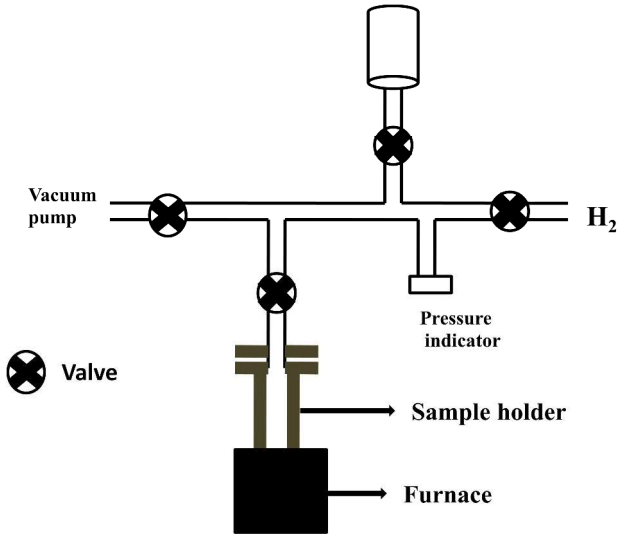

Fig.1 Schematic of Sievert's apparatus

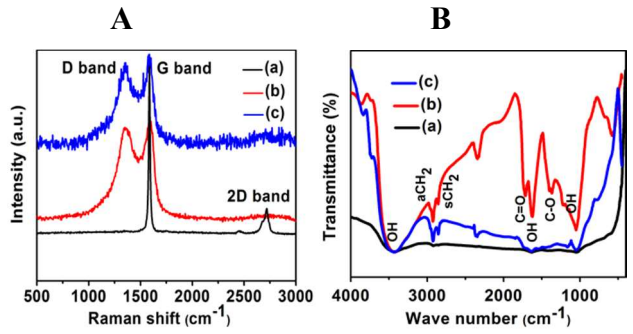

Fig.2A Raman spectra of (a) graphite, (b) GO and (c) HEG, 2B FTIR spectra of (a) graphite, (b) GO and(c) HEG

was loaded for the measurement. The residual impurities were removed by degassing the sample in vacuum environment at 200°C for a time period of 2 hours prior to the measurement. At high pressures, van der Waals correction factors such as $a=2.48\times10^{-2}$ Pa m^6/mol^2 and $b=2.66\times10^{-5}$ m^3/mol for hydrogen have been applied to the ideal gas equation. Schematic of Sieverts apparatus is shown in Fig. 1.

5. Results and discussion

Raman spectroscopy is a well known tool for characterization of graphene. Fig. 2A (a–c) shows the Raman spectra of graphite, GO and HEG respectively. D band at 1350 cm^{-1}, the breathing mode of κ-point phonons with A_{1g} symmetry is attributed to the defects or disorder. The presence of peak at 2717 cm^{-1} is the overtone of the G band called 2D band. G band corresponds to the E_{2g} mode of sp^2 carbon atoms at 1584 cm^{-1}[33-35]. Absence of D band in Fig. 2A (a) indicates that graphite is defect free. High intense D bands in GO and HEG says that defects can be induced on graphite by oxidation and on HEG by exfoliation of GO. Functional groups in graphite, GO and HEG were identified by FTIR analysis. Fig. 2B (a -c) shows the FTIR spectra of Graphite, GO and HEG respectively. In Fig. 2B (a), broad peak centered at 3454 cm^{-1} and 1624 cm^{-1} were assigned to the stretching vibrations of OH functional groups. The peaks at 2924 cm^{-1} and 2858 cm^{-1} were assigned to the symmetric and anti symmetric stretching vibrations of $–CH_2$ [36]. In Fig. 2B (b), broadening of peaks at 3454 cm^{-1} and at l624 cm^{-1} indicates that GO samples contain more OH groups [37]. Peaks at 1725 cm^{-1} and 1390 cm^{-1} attributed to C=O and C–O, stretching vibrations of COOH [38]. After exfoliation, Intensities of peaks correspond to –OH functional group (3454 cm^{-1}, 1624 cm^{-1}), C=O (1725cm^{-1}), C–O

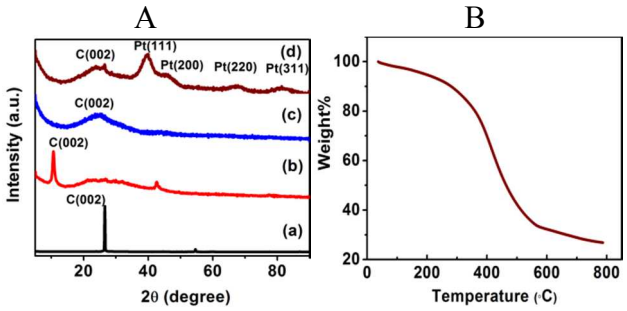

Fig. 3A XRD of (a) graphite, (b) GO, (c) HEG and (d) Pt-HEG, 3B TGA of Pt-HEG

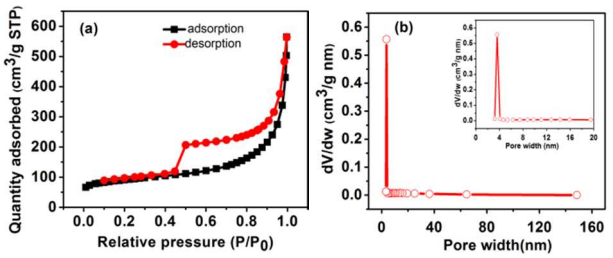

Fig. 4(a) Nitrogen adsorption-desorption isotherm and (b) pore-size distribution for Pt-HEG

(1370 cm^{-1}) and –OH (1390 cm^{-1}) of COOH were drastically reduced (Fig. 2B (c)) [39], The peaks at 2924 cm^{-1} and 2858 cm^{-1} indicates the vibrations of $–CH_2$ [40].

Structural identification was done by XRD analysis. XRD patterns were recorded for graphite, GO, HEG and Pt-HEG are shown in Fig. 3A (a-d). Graphite, GO and HEG shows distinct XRD pattern. The intense crystalline peak (002) at 2θ=26.5° (Fig. 3A (a)) is attributed to the plane of hexagonal graphite with a d spacing of 0.34 nm. This peak indicates the presence of long range order and crystalline nature of hexagonal graphite. Shift of peak corresponds to (002) plane towards 2θ=10° is observed in Fig. 3A (b) when the graphite is converted to graphite oxide. Exfoliation of GO is confirmed by the reappearance of (002) broad peak centered around 24 ° (Fig. 3A(c)). The broadening indicates the loss of long range order in few layered HEG, which is a basic characteristic of graphene. Intense peaks at 2θ= 39.7°, 46.2°, 67.4° and 81.2° (Fig. 3A(d)) are the reflection planes of fcc structure of crystalline platinum (JCPDS 04-0802).

Platinum loading was estimated from TGA. Fig. 3B shows the TGA curve of Pt-HEG. TGA was carried out in air atmosphere within a temperature range of room temperature to 800 °C. The weight loss below 200 °C was due to water content as well as residual EG remaining on the sample. When the temperature was increased further, residual functional groups were removed. Since the carbon material was oxidized completely below 700 °C, the residue remaining after 700 °C was Pt.

BET surface area and porosity were examined through nitrogen adsorption and desorption. Fig. 4(a and b) shows the nitrogen adsorption-desorption isotherms and BJH pore-size distribution for Pt-HEG. Isotherm looks like type IV as per IUPAC nomenclature. BET specific surface area obtained for Pt-HEG is 298 m^2/g. BJH pore distribution says that maximum number of pores have size of 3.6 nm, which indicates mesoporous

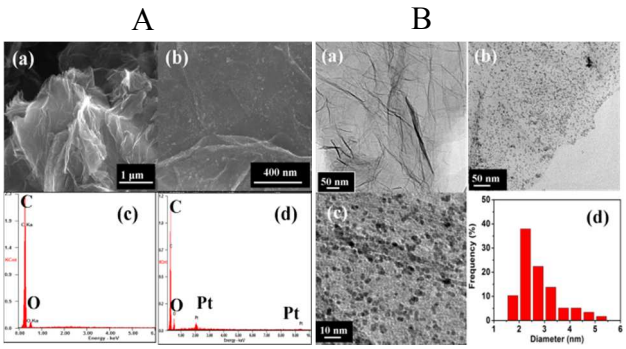

Fig. 5A (a) FESEM image of HEG, (b) FESEM image of Pt-HEG, (c and d) EDX of HEG and Pt/HEG, 5B (a) TEM image of HEG, (b)TEM image of Pt/HEG, (c) HRTEM image of Pt/HEG and (d) particle size histogram of Pt/HEG

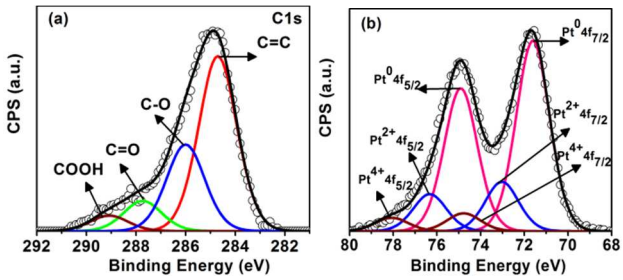

Fig.6(a) Deconvoluted C1s peak and (b) Deconvoluted Pt 4f peak of Pt-HEG

characteristic of HEG.

FESEM and TEM imaging revealed morphological features. Fig. 5A (a and b) shows the typical FESEM images of HEG and Pt/HEG. HEG contains highly wrinkled architecture with few layers. This structural feature was further confirmed by TEM analysis (panel a in Fig. 5B). Energy dispersive X-ray (EDX) analysis spectra of HEG and Pt/HEG recorded are shown in Fig. 5A (c and d). EDX spectra indicated the presence of carbon and oxygen in HEG (Fig. 5A(c)), presence of carbon, oxygen and platinum in Pt-HEG (Fig. 5A(d)). The element oxygen was due to the presence of oxygen containing functional groups. Decoration of Pt nanoparticles over HEG was confirmed from the FESEM (panel b of Fig. 5A) and TEM images of Pt/HEG displayed in Fig. 5B (b and c). Size distribution of Pt particles on HEG is shown in Fig. 5B(d).

Further, XPS measurement was performed to detect the composition of Pt-HEG. XPS peak fit analysis was carried out using casa XPS software. Fig. 6(a) shows the deconvoluted C1s spectra of Pt/HEG. The binding energies were calibrated with respect to C1s peak at 284.7 eV [41]. The peak positions of C-O, C=O and COOH for Pt-HEG are at 286 eV, 287.7eV and 289.1eV [42] respectively. Platinum 4f core-level spectrum of Pt-HEG was de convoluted in to three pairs of doublets are shown in Fig. 6(b). The peaks observed at 71.6 and 74.9 eV indicates Pt exist in zero valent metallic state [43]. The second pair of doublets at 73.1 and 76.4 eV were assigned to to +2 oxidation state of platinum. The doublets observed at 74.8 and 78.1 eV were assigned to to +4 oxidation state of platinum.[44, 45].

High pressure hydrogen adsorption-desorption measurement was done for Pt-HEG. Fig. 7 (a) shows the hydrogen adsorption isotherms of Pt-HEG at different temperature and pressures. The isotherms were nearly linear. Pt/HEG shows a maximum hydrogen adsorption capacity of 1.4wt % at 25 °C and 3MPa pressure. Hydrogen storage capacity of pristine HEG reported by vinayan et al [2] is 0.5 wt% at 25 °C and 2 MPa, while Pt-HEG (present work) shows 1 wt% at 2 MPa and 25 °C. Hydrogen

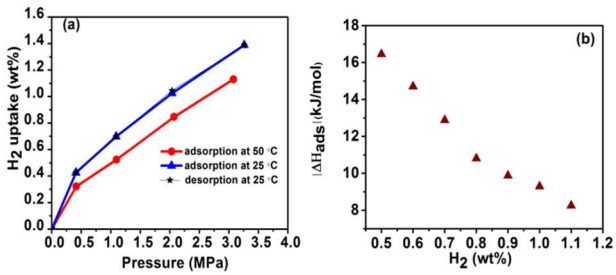

Fig.7 (a) Hydrogen adsorption-desorption isotherms of Pt-HEG and (b) isosteric heat of adsorption for Pt-HEG

Table 1 Hydrogen uptake capacity of different materials.

Material	Hydrogen uptake capacity
HEG	0.5wt% at 2MPa and 298K[2]
Pt-HEG	1 wt% at 2 Mpa and 298K (present study)
Gr	0.067 wt% at 303 K and 5.7 Mpa[26]
Gr-Pt	0.15 wt% at 303 K and 5.7 Mpa[26]
Pt nanoparticles doped on superactivated carbon (Pt/AX-21)	1.2 wt% at 10 MPa and 298K[46]
Pt doped ordered mesoporous carbon	1.49 wt% at 30 MPa and 298K[47]

uptake capacity of Pt-HEG surpasses that of HEG[2], graphene (Gr) [26], Pt-Gr [26], Pt nanoparticles doped superactivated carbon[46], Pt doped ordered mesoporous carbon[47]. For clarity, details are shown in table1.

The isosteric heat of adsorption $|\Delta H_{ads}|$ was calculated from the adsorption isotherms using the equation

$$|\Delta H_{ads}| = -R\left(\frac{\partial \ln P}{\partial (1/T)}\right) \qquad (1)$$

where, $|\Delta H_{ads}|$ is the isosteric heat of adsorption and R is the ideal gas constant. High pressure hydrogen adsorption isotherms recorded at 25 °C and 50 °C was used for calculating the isosteric heat of adsorption. Fig. 7(b) shows the variation of estimated isosteric heat of adsorption with adsorption amount. Isosteric heat of adsorption reported for pristine HEG at 0.6 wt% and 0.7 wt% are 6.78 kJ/mol and 6.03 kJ/mol respectively [2], Pt-HEG exhibits 14.7 kJ/mol at 0.6 wt%, which is higher than that of HEG.

Carbon based materials with high surface area and appropriate pore size are well-known for hydrogen storage by physisorption and the interaction between hydrogen and host material is weak van-der Waals forces. Carbon based materials cannot meet the operational targets at ambient temperature due to its low heat of adsorption. Hydrogen spillover has been proposed to enhance the storage capacity of carbon-based nanostructures at room temperature. First, Hydrogen molecules interact with catalyst particles and dissociate in to hydrogen atoms. H atoms then migrate from the catalyst particles to the receptor material and further diffuse throughout the entire receptor [48]. Here Pt acts as the catalyst for H_2 dissociation and HEG is the receptor. The high adsorption capacities as well as heat of adsorption of Pt-HEG in comparison to HEG are direct evidences to spill over of hydrogen.

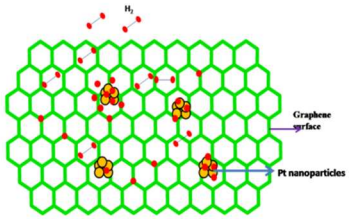

Fig.8 Schematic of Hydrogen spill over in Pt-HEG

H/Pt ratio for platinum of approximately 3 nm is 0.35 [49]. For Pt/HEG at 3MPa and room temperature, 71% of the hydrogen uptake is by HEG. Optimization of the Pt loading may help to improve the hydrogen uptake. Schematic of hydrogen spillover in Pt-HEG is shown in Fig.8.

Conclusions

In summary, we have investigated the existence of Pt-HEG as hydrogen adsorbent. HEG was obtained from GO by hydrogen exfoliation technique. Polyol reduction method was used to disperse platinum on HEG. We estimated the hydrogen adsorbed on Pt-HEG at elevated temperatures and moderate pressures, provided direct evidence to hydrogen spill over. By spill over, adsorption capacity was enhanced by a factor of two at 298K and 2 MPa in comparison to HEG. The overall isosteric heat of adsorption of hydrogen in Pt-HEG lies in the range of 17-8 kJ/mol. Our results revealed the feasibility of Pt-HEG as a practical light-weight hydrogen storage material.

Acknowledgement

The authors wish to thank IIT madras for supporting this work and SAIF IIT Madras FTIR measurement. Divya P. is thankful to the CSIR (Council of Scientific and Industrial Research), India for SRF assistance.

Notes and references

[a] *Address, Address, Town, Country. Fax: XX XXXX XXXX; Tel: XX XXXX XXXX; E-mail: xxxx@aaa.bbb.ccc*

† Electronic Supplementary Information (ESI) available: []. See DOI: 10.1039/b000000x/

‡

1. S. K. Bhatia and A. L. Myers, *Langmuir*, 2006, **22**, 1688-1700.
2. V. B. Parambhath, R. Nagar, K. Sethupathi and S. Ramaprabhu, *The Journal of Physical Chemistry C*, 2011, **115**, 15679-15685.
3. A. C. Dillon, K. M. Jones, T. A. Bekkedahl, C. H. Kiang, D. S. Bethune and M. J. Heben, *Nature*, 1997, **386**, 377-379.
4. Y. Ye, C. C. Ahn, C. Witham, B. Fultz, J. Liu, A. G. Rinzler, D. Colbert, K. A. Smith and R. E. Smalley, *Applied Physics Letters*, 1999, **74**, 2307-2309.
5. M. Rzepka, E. Bauer, G. Reichenauer, T. Schliermann, B. Bernhardt, K. Bohmhammel, E. Henneberg, U. Knoll, H.-E. Maneck and W. Braue, *The Journal of Physical Chemistry B*, 2005, **109**, 14979-14989.
6. J. S. Noh, R. K. Agarwal and J. A. Schwarz, *International Journal of Hydrogen Energy*, 1987, **12**, 693-700.
7. Y. Sun, L. Wang, W. Amer, H. Yu, J. Ji, L. Huang, J. Shan and R. Tong, *J Inorg Organomet Polym*, 2013, **23**, 270-285.
8. J. Weitkamp, M. Fritz and S. Ernst, *International Journal of Hydrogen Energy*, 1995, **20**, 967-970.
9. V. Tozzini and V. Pellegrini, *Physical Chemistry Chemical Physics*, 2013, **15**, 80-89.
10. P. Sessi, J. R. Guest, M. Bode and N. P. Guisinger, *Nano Letters*, 2009, **9**, 4343-4347.
11. V. Tozzini and V. Pellegrini, *The Journal of Physical Chemistry C*, 2011, **115**, 25523-25528.
12. R. Balog, B. Jørgensen, J. Wells, E. Lægsgaard, P. Hofmann, F. Besenbacher and L. Hornekær, *Journal of the American Chemical Society*, 2009, **131**, 8744-8745.
13. K. S. Subrahmanyam, P. Kumar, U. Maitra, A. Govindaraj, K. P. S. S. Hembram, U. V. Waghmare and C. N. R. Rao, *Proceedings of the National Academy of Sciences*, 2011, **108**, 2674-2677.
14. Y. Okamoto and Y. Miyamoto, *The Journal of Physical Chemistry B*, 2001, **105**, 3470-3474.

15. V. V. Ivanovskaya, A. Zobelli, D. Teillet-Billy, N. Rougeau, V. Sidis and P. R. Briddon, *Eur. Phys. J. B*, 2010, **76**, 481-486.
16. Y. Miura, H. Kasai, W. Diño, H. Nakanishi and T. Sugimoto, *Journal of Applied Physics*, 2003, **93**, 3395-3400.
17. S. Casolo, O. M. Løvvik, R. Martinazzo and G. F. Tantardini, *The Journal of Chemical Physics*, 2009, **130**, -.
18. S. Goler, C. Coletti, V. Tozzini, V. Piazza, T. Mashoff, F. Beltram, V. Pellegrini and S. Heun, *The Journal of Physical Chemistry C*, 2013, **117**, 11506-11513.
19. S. Patchkovskii, J. S. Tse, S. N. Yurchenko, L. Zhechkov, T. Heine and G. Seifert, *Proceedings of the National Academy of Sciences of the United States of America*, 2005, **102**, 10439-10444.
20. B. H. Kim, W. G. Hong, H. Y. Yu, Y.-K. Han, S. M. Lee, S. J. Chang, H. R. Moon, Y. Jun and H. J. Kim, *Physical Chemistry Chemical Physics*, 2012, **14**, 1480-1484.
21. G. Srinivas, Y. Zhu, R. Piner, N. Skipper, M. Ellerby and R. Ruoff, *Carbon*, 2010, **48**, 630-635.
22. C. Ataca, E. Aktürk, S. Ciraci and H. Ustunel, *Applied Physics Letters*, 2008, **93**, -.
23. H. Lee, J. Ihm, M. L. Cohen and S. G. Louie, *Nano Letters*, 2010, **10**, 793-798.
24. L. Wang, K. Lee, Y.-Y. Sun, M. Lucking, Z. Chen, J. J. Zhao and S. B. Zhang, *ACS Nano*, 2009, **3**, 2995-3000.
25. F. M. P. Z. M. Ao, *Physical Review B*, 2010, **81**, 205406
26. C.-C. Huang, N.-W. Pu, C.-A. Wang, J.-C. Huang, Y. Sung and M.-D. Ger, *Separation and Purification Technology*, 2011, **82**, 210-215.
27. B. P. Vinayan, R. Nagar and S. Ramaprabhu, *Journal of Materials Chemistry A*, 2013, **1**, 11192-11199.
28. V. B. Parambhath, R. Nagar and S. Ramaprabhu, *Langmuir*, 2012, **28**, 7826-7833.
29. S. Nachimuthu, P.-J. Lai and J.-C. Jiang, *Carbon*, 2014, **73**, 132-140.
30. H.-Y. Wu, X. Fan, J.-L. Kuo and W.-Q. Deng, *The Journal of Physical Chemistry C*, 2011, **115**, 9241-9249.
31. W. S. Hummers and R. E. Offeman, *Journal of the American Chemical Society*, 1958, **80**, 1339-1339.
32. A. Kaniyoor, T. T. Baby and S. Ramaprabhu, *Journal of Materials Chemistry*, 2010, **20**, 8467-8469.
33. A. C. Ferrari and J. Robertson, *Physical Review B*, 2000, **61**, 14095-14107.
34. D. Graf, F. Molitor, K. Ensslin, C. Stampfer, A. Jungen, C. Hierold and L. Wirtz, *Nano Letters*, 2007, **7**, 238-242.
35. F. Tuinstra and J. L. Koenig, *The Journal of Chemical Physics*, 1970, **53**, 1126-1130.
36. Z. L. X. Sun, K. Welsher, J. T. Robinson, A. Goodwin, S. Zaric and H. Dai, *Nano Research*, 2008, **1**, 203.
37. G. I. Titelman, V. Gelman, S. Bron, R. L. Khalfin, Y. Cohen and H. Bianco-Peled, *Carbon*, 2005, **43**, 641-649.
38. H.-K. Jeong, L. Colakerol, M. H. Jin, P.-A. Glans, K. E. Smith and Y. H. Lee, *Chemical Physics Letters*, 2008, **460**, 499-502.
39. W. Gao, L. B. Alemany, L. Ci and P. M. Ajayan, *Nat Chem*, 2009, **1**, 403-408.
40. G. Wang, B. Wang, J. Park, J. Yang, X. Shen and J. Yao, *Carbon*, 2009, **47**, 68-72.
41. B. Luo, S. Xu, X. Yan and Q. Xue, *Journal of The Electrochemical Society*, 2013, **160**, F262-F268.
42. A. Kaniyoor, T. T. Baby, T. Arockiadoss, N. Rajalakshmi and S. Ramaprabhu, *The Journal of Physical Chemistry C*, 2011, **115**, 17660-17669.
43. F. Şen and G. Gökağaç, *The Journal of Physical Chemistry C*, 2007, **111**, 5715-5720.
44. J. Wang, G. Yin, Y. Shao, S. Zhang, Z. Wang and Y. Gao, *Journal of Power Sources*, 2007, **171**, 331-339.
45. F. Su, Z. Tian, C. K. Poh, Z. Wang, S. H. Lim, Z. Liu and J. Lin, *Chemistry of Materials*, 2009, **22**, 832-839.
46. Y. Li and R. T. Yang, *The Journal of Physical Chemistry C*, 2007, **111**, 11086-11094.
47. D. Saha and S. Deng, *Langmuir*, 2009, **25**, 12550-12560.
48. H. Cheng, L. Chen, A. C. Cooper, X. Sha and G. P. Pez, *Energy & Environmental Science*, 2008, **1**, 338-354.
49. J, W. Ohizumi, A. Oya, M. J. Illan-Gomez, M. C. Roman-Martinez and A. Linares-Solano, *Carbon*, 2000, **38**, 778-780.